Catalysis Today 145 (2009) 294–299

Contents lists available at ScienceDirect

Catalysis Today

journal homepage: www.elsevier.com/locate/cattod

Hard X-ray photon-in photon-out spectroscopy

Pieter Glatzel [a,*], Marcin Sikora [a], Grigory Smolentsev [b], Marcos Fernández-García [c]

[a] European Synchrotron Radiation Facility (ESRF), BP22, 6 rue Jules Horowitz, 38043 Grenoble, France
[b] Faculty of Physics and Center for Nanoscale Structure of Matter, Southern Federal University, Rostov-on-Don, Russia
[c] Instituto de Catalisis y Petroleoquimica, CSIC, C/Marie Curie s/n, 28049 Madrid, Spain

ARTICLE INFO

Article history:
Available online 21 December 2008

PACS:
61.10.Ht
87.64.Fb
87.64.Gb
71.70.Ch

Keywords:
Emission spectroscopy
Electronic structure
EXAFS
RIXS

ABSTRACT

Spectroscopic techniques to study the electron configuration and local coordination of a central atom by detecting inner-shell radiative decays following photoexcitation using hard X-rays are presented. The experimental setup requires an X-ray spectrometer based on perfect crystal Bragg optics. The possibilities arising from non-resonant and resonant X-ray emission spectroscopy are discussed when the instrumental energy broadenings of the primary (beamline) monochromator and the crystal spectrometer for X-ray emission detection are on the order of the core hole lifetimes of the intermediate and final electronic states. The small energy bandwidth in the emission detection yields line-sharpened absorption features. In transition metal compounds, electron–electron interactions as well as orbital splittings and fractional population can be revealed. Combination with EXAFS spectroscopy enables to extend the *k*-range beyond unwanted absorption edges in dilute samples that limit the EXAFS range in conventional absorption spectroscopy.

1. Introduction

Photon-in photon-out techniques are targeted at applications where the sample environment cannot be chosen freely, i.e. UHV conditions suitable for photoemission experiments are not possible. This applies in particular to catalysis research where the aim is to study the catalyst under working conditions. The most popular *in situ* X-ray spectroscopy technique to study the element-specifically electronic structure and local coordination is X-ray absorption spectroscopy (XAS) [1,2]. The X-ray absorption near edge structure (XANES) is often used to obtain oxidation states but XANES also contains information on the local geometry and coordination. A detailed analysis of the XANES structure is a complex task because of the numerous interactions that contribute to its shape. The spectroscopy using the extended absorption range (EXAFS) is well developed theoretically and experimentally but the technique has its inherent limitations (e.g. differentiation of elements close in atomic number) and the ideal experimental conditions (e.g. sample thickness, homogeneity) for a correct EXAFS analysis are not always given. It is thus desirable to introduce other X-ray techniques that either provide a means to verify the results obtained from XAS or yield additional information concerning local coordination and electronic structure.

An X-ray absorption spectrum arises from excited states that subsequently decay either non-radiatively by emitting an electron (Auger decay) or radiatively (fluorescence). The fluorescence or, more general, the X-ray emission exhibits a chemical sensitivity when recorded with an instrumental energy bandwidth that is on the order of the lifetime broadenings [3–5]. The required energy resolution can be achieved by employing an X-ray emission spectrometer based on perfect-crystal Bragg optics (Fig. 1) [6–8].

High-brilliance, tunable X-ray sources that are nowadays available allow to study the X-ray emission with unprecedented energy resolution and sensitivity resulting in a wealth of new applications [3]. The emission spectrometer installed at a synchrotron radiation beamline acts as a secondary monochromator for the emitted X-rays with an instrumental energy broadening that is similar to the primary crystal monochromator that selects the incident energy. Non-resonant X-ray emission spectroscopy (XES) provides information on occupied electron orbitals in the valence shell. By tuning the incident energy to an absorption edge, i.e. to a resonant state, and observing the X-ray emission one takes advantage of the properties of resonant X-ray emission (RXES) or resonant inelastic X-ray scattering (RIXS) [5,9]. As a result, a spectral sharpening occurs that can reveal previously unobserved features giving valuable input for a detailed analysis.

The main strength of XES is that the electronic structure can be studied element-selectively and under *in situ* conditions. XES is thus complementary to XAS which mainly addresses the local coordination (EXAFS) or provides only basic information on the

* Corresponding author.
E-mail address: Glatzel@esrf.fr (P. Glatzel).

0920-5861/$ – see front matter © 2008 Elsevier B.V. All rights reserved.
doi:10.1016/j.cattod.2008.10.049

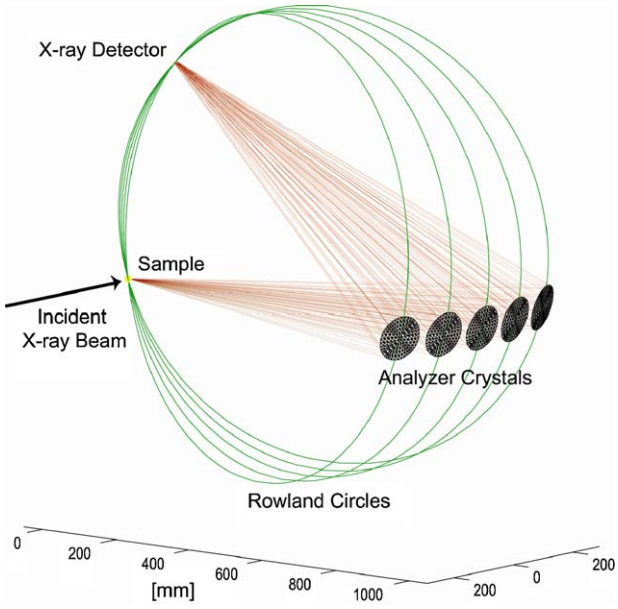

Fig. 1. X-ray emission spectrometer with vertical scattering geometry employing five analyzer crystals. The focusing (Rowland) circles are shown.

electronic structure, e.g. an oxidation or reduction of the metal. The activity of catalytic sites and reaction kinetics depend on the electronic structure and the potential of X-ray emission spectroscopy to study chemical reactions is considerable. The aim of this contribution is therefore to give an overview of the technique and we hope to give some ideas for experiments to the inclined reader. The paper is organized as follows. We first outline some basic aspects of resonant and non-resonant XES. We then give examples that demonstrate the possibilities of XES. This section is divided into non-resonant XES, i.e. fluorescence lines, and resonant XES (RXES or RIXS).

2. X-ray emission spectroscopy with lifetime resolution

The energy level diagram in Fig. 2 schematically describes the energy levels that are involved in absorption and emission spectroscopy. We use a multi-electron scheme where the vertical axis denotes the total energy of the entire system including all electrons that are possibly involved in the photoabsorption process. An absorption edge is formed by discrete resonances (e.g. 3d transition metal K pre-edges) as well as broad excitations

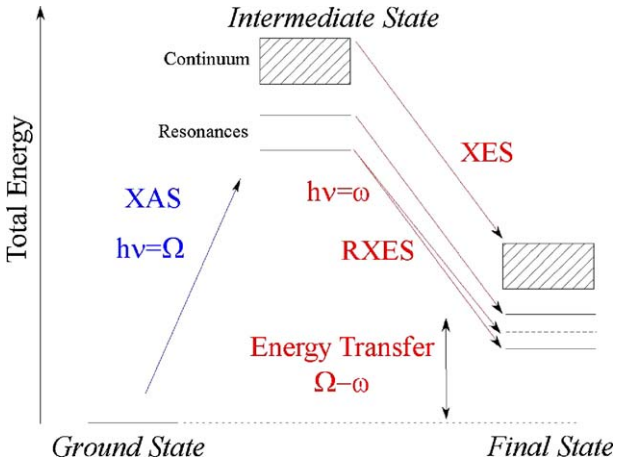

Fig. 2. Energy scheme for X-ray absorption and emission.

into a band or the continuum. A radiative decay from a continuum state gives rise to a non-resonant X-ray emission or fluorescence line. We define high-energy-resolution X-ray emission measurements as detecting the fluorescence line with an energy bandwidth on the order or below the core hole lifetime broadening.

The physics involved in a two-level photon scattering process (second-order optical process) are described by the Kramers–Heisenberg equation [9]. The scattered X-ray intensity is a function of two experimental energies, the incident X-ray energy Ω and emitted X-ray energy ω, as well as the energies of the electronic configurations. It is useful to define the energy transfer Ω–ω in order to relate the energies of all intermediate and final states to the same reference energy, i.e. the ground state energy.

The model energy diagram in Fig. 2 shows two resonant intermediate states of which the lower decays into two final states. The final state that is represented by a dashed line is due to the so-called final state effects. These are electron interactions that occur only in the final and not in the intermediate state. We now translate this energy diagram into a contour plot where the incident energy points along the horizontal axis and the energy transfer or final state energy points along the vertical direction (Fig. 3). Comparisons between different spectra and a quantitative analysis are usually made for line plots. We therefore show some possibilities for extracting line plots from the full RIXS plane. When the incident energy is plotted versus the energy transfer, both lifetime broadenings extend perpendicularly to each other in the RIXS plane. The broader intermediate state lifetime stretches along the incident energy axis. Scans of the emission energy (constant incident energy scans) yield spectra that are broadened by the final state lifetime broadening that is usually smaller than for the intermediate state.

It is important to note that terminology like "lifetime suppressed" that is sometimes found in the literature does not mean that the lifetime broadenings are reduced or even disappear in resonant spectroscopies. The lifetime broadenings are always there as the RIXS plane shows (Fig. 3). All the experimentalist can do (apart from de-convoluting the spectra [10]) is scan through the RIXS plane such that the line broadening is minimized. This is in many cases achieved using a diagonal cut through the RIXS plane as shown in Fig. 3. Experimentally, this means that the emission energy is fixed while the incident energy is scanned (constant emission energy scan). This resembles an absorption scan and was done by Hämäläinen et al. on dysprosium [11].

A comparison between an absorption and a constant emission energy scan requires some further discussion. First, the constant emission energy scan shows a feature at 4969 eV which is absent in the absorption scan. One may be led to conclude that the reduced lifetime broadening reveals this absorption feature. While this feature is indeed revealed by using an instrumental energy bandwidth below the lifetime broadening there is, however, no absorption resonance at 4969 eV. This may appear counter-intuitive since the intermediate states are reached via absorption of a photon. Comparison of the RIXS plane with the energy diagram in Fig. 2 shows that, in fact, the feature at 4969 eV is due to the absorption resonance at 4968 eV that causes via the final state effect and the lifetime broadening a peak at higher incident energy. The limitations in interpretation of constant emission scans as absorption scans have been pointed out by Carra et al. [12] as well as Loeffen et al. [10]. Secondly, the pre-edge features show a stronger intensity relative to the main edge in the high-resolution scan. This has also been observed experimentally in Fe systems [13,14].

The fact that the lifetime broadenings do not disappear in RIXS spectroscopy has important ramifications. A large number of resonant states with an energy splitting that is considerably smaller than their intermediate and final state lifetime broadenings cannot

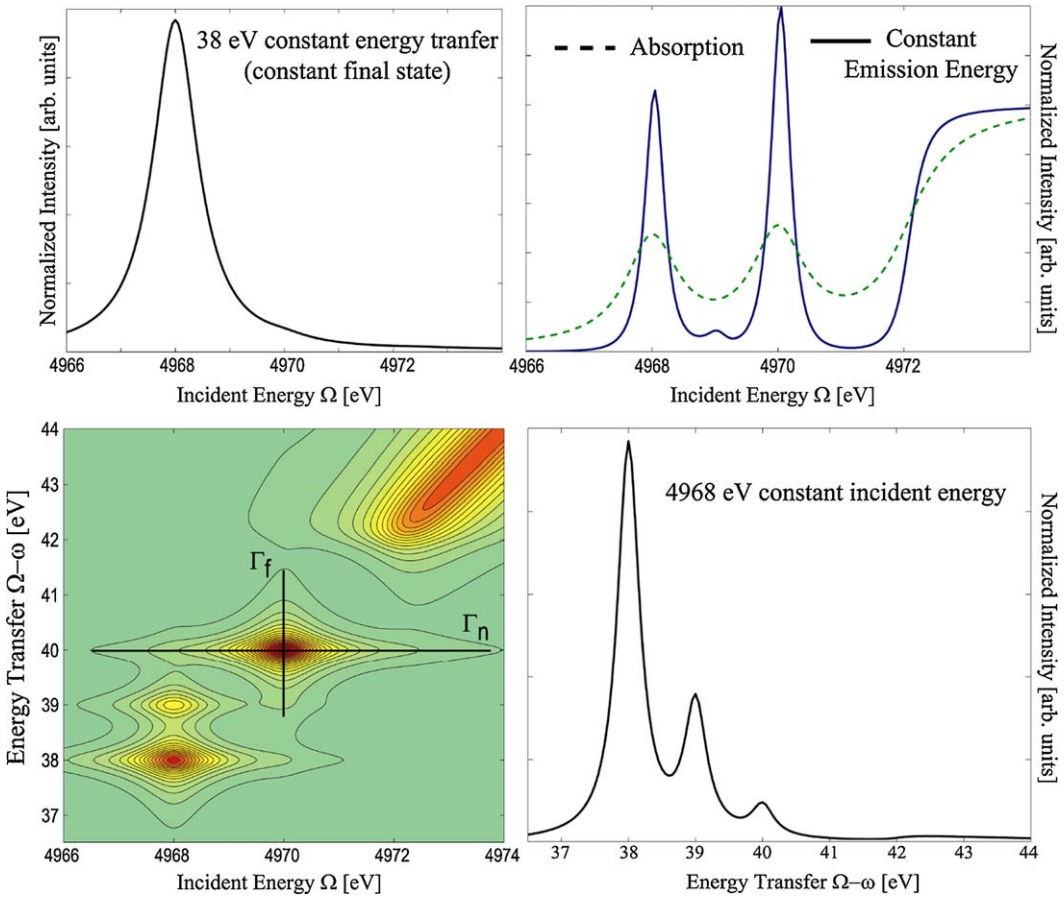

Fig. 3. Bottom left: RIXS plane for the model system in Fig. 2. The lifetime broadenings Γ_n and Γ_f for the intermediate and final state, respectively, are indicated. Top left and bottom right: line scans obtained from the RIXS plane at constant final state and constant incident energy. Top right: constant emission energy scan (diagonal cut through RIXS plane) compared to the absorption spectrum.

be well resolved in RIXS. There is thus a limit to the line sharpening effect due to the lifetime broadenings that may cause overlap between resonances that are close in energy.

We can reduce the energy transfer to just a few eV. The energy scale in a RIXS spectrum then coincides with UV–Vis absorption spectroscopy. Indeed, the RIXS process allows to observe excitations of a few eV probed by hard X-rays and with the advantage of element-selectivity. The excitations are reached via a two-photon process and thus excitations that are not observable in UV–Vis spectroscopy can be reached, e.g. dd excitations [15]. However, these are low count rate experiments that require high incident X-ray flux and a large solid angle spectrometer.

3. Non-resonant XES

We discuss in the following emission spectra that arise from transitions between the continuum states in Fig. 2. With the excitation energy set well above (>30 eV) an absorption edge the X-ray emission spectrum is independent of the incident energy if we neglect weak multi-electron excitations. The emitted X-rays after non-resonant excitations are generally referred to as fluorescence lines. The chemical dependence of the Kβ lines in 3d transition metals has been discussed by many authors [4,5]. They can be separated into the Kβ main lines ($K\beta_{1,3}$ and Kβ′) that arise from a 3p to 1s transition and the Kβ satellite lines or valence-to-core transitions just below the Fermi level. The Kβ main lines reflect the valence shell spin state and thus enable to detect oxidation state changes as well as high-spin–low-spin transitions.

It is interesting to note that the Kβ main line shape mainly depends on the electronic structure and is hardly sensitive to the local structure [16]. The Kβ main lines reflect the local coordination only indirectly, for example when a structural change results in a spin transition. This is in contrast to the XANES in 3d transition metals that is strongly influenced by the atomic structure. Combined measurement of the Kβ main lines and XANES thus helps to disentangle structural from electronic changes.

The Kβ satellite lines in 3d transition metals arise from valence-to-core transitions and thus show a very strong chemical dependence. In particular, they show a strong sensitivity to the type of ligand. Unlike XAS, the XES shows distinct signatures for different ligands that enable to identify the quality of the chemical environment (Fig. 4). For example, nitrogen and oxygen ligands can be clearly distinguished [17]. Safonov et al. used the technique to characterize the Cr ligands in electroplated Cr when organic substances are present in the electrolyte [18]. Also, ligand protonation yields spectral changes that can be assigned to, e.g. OH^- or H_2O groups. The sensitivity of valence-to-core XES on the degree of ligand protonation has been proposed by Bergmann and Penner-Hahn in Zn containing coordination complexes and proteins [19]. The spectral signature does not depend strongly on the bond distances and angles in contrast to the X-ray absorption features. It is thus easier to assign a spectral feature to a change in the ligand environment. The technique is thus a tool complementary to EXAFS.

The Kβ satellite spectral features can be calculated using the FEFF code or density functional theory (DFT). It appears that for many systems ground state calculations are sufficient because the

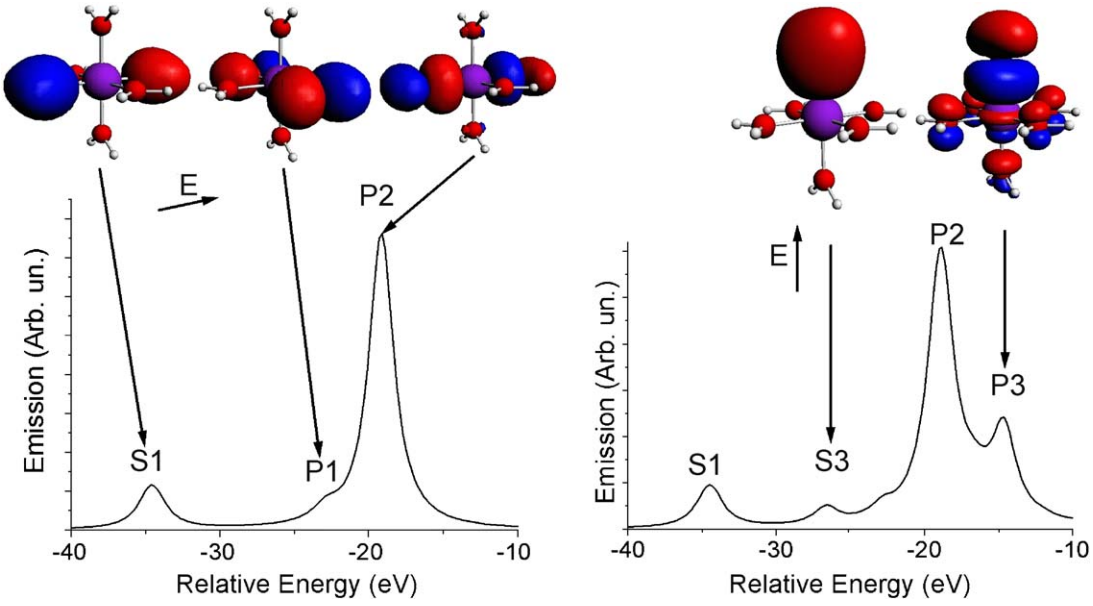

Fig. 4. Kβ satellite lines for model systems $[Mn(H_2O)_6]^{2+}$ (left) and $[Mn(H_2O)_5NH_2]^{+}$ (right). Replacement of one H_2O ligand by NH_2 lowers the symmetry and yields additional peaks.

valence orbitals that take part in the transition are strongly screened from the core hole potential. Thus, valence-to-core XES can be readily modeled using ground state DFT calculations. Using DFT it is possible to visualize the molecular orbitals and assign them to spectral features. This provides an important tool for spectral interpretation that will help to understand the effect of changes in the ligand environment on the electronics structure. When interpreting the spectra it is important to be aware of possible multi-electron transitions. Their intensities depend on the incident energy and it is thus possible to identify them in the Kβ satellite spectrum [20].

4. High-resolution XAS

Fluorescence detected absorption spectroscopy was developed in order to be able to measure dilute samples that do not absorb enough photons to obtain a XAS spectrum in transmission mode. XAS in fluorescence mode is detected either without energy resolution (e.g. photodiode) or with energy resolution (e.g. Ge detector). The better the energy resolution, i.e. the smaller the energy bandwidth around the fluorescence line, the better will be the signal to background ratio. The limit for improvement is set by the core hole lifetime broadening because a smaller bandwidth in the emission detection will not significantly improve the signal to background ratio anymore. We denote an absorption scan that is recorded by detecting a fluorescence line with an instrumental energy bandwidth on the order of the core hole lifetime broadening as high-energy-resolution fluorescence detected (HERFD) XAS. Apart from the advantage of having the best possible signal to background ratio, emission detection with lifetime resolution also yields line-sharpened absorption features [21–24]. Fig. 5 shows that the effect is very pronounced for high-Z materials (e.g. W, Pt, Au, ...).

We have shown (*vide supra*) that such a scan, a constant emission energy scan, can be deceptive in the region of resonant excitations because it may show features that are not actual absorption features. One has to be sure that final state effects in resonant excitation close to the Fermi level as they are shown by the dashed line in Fig. 2 are absent. This can be verified by first recording a full resonance plane as shown in Fig. 3 before performing HERFD XAS measurements. The delocalized character of the 5d electrons ensures that final state effects are negligible for the fifth row transition metals. A constant emission energy scan that employs the $L\alpha_1$ fluorescence line thus becomes a very good approximation to an absorption scan. This can be verified by theoretical calculations. The FEFF code allows to adjust the core hole lifetime broadening and the experimental results can be verified immediately [25]. This has been shown by de Groot et al. as well as Safonova et al. on Pt and van Bokhoven et al. on Au [21–23]. We note that the condition of weak final state interactions is only in few cases fulfilled for the K fluorescence lines of 3d transition metal complexes. The technique nevertheless yields sharper spectral features but care has to be taken in these systems when analyzing the data.

We note that alternatively it is possible to apply a mathematical procedure (deconvolution) to obtain an absorption spectrum that

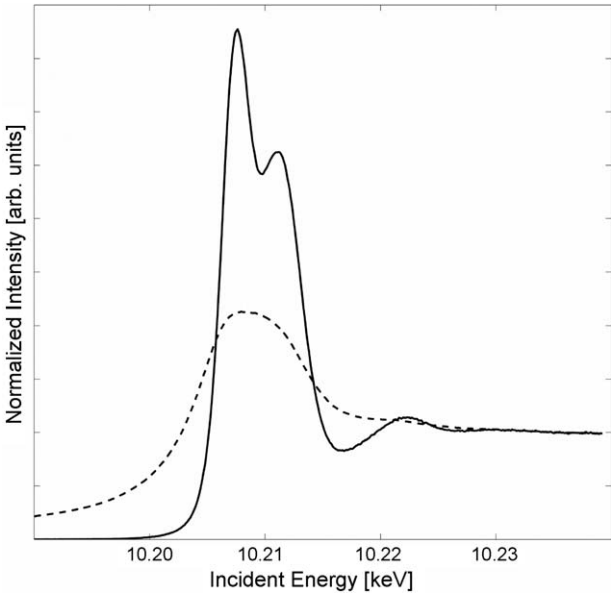

Fig. 5. Total fluorescence yield (dotted line) and HERFD (solid line) XAS at the W L_3-edge of a anatase-type Ti–W mixed oxide (W content; 2 atm%).

is not broadened by the core hole lifetime. This has been demonstrated by Loeffen et al. at the L_3-edges of rare earths [10]. A deconvolution has the advantage that it can be applied directly to a transmission detected absorption spectrum and no emission spectrometer is necessary. HERFD XAS has the advantage that no data treatment is necessary and with new large solid spectrometers the technique is applicable to dilute samples that cannot be measured in transmission mode.

The fact that HERFD XAS fully separates most fluorescence lines can be used to record extended absorption scans beyond unwanted edges that occur either in transmission or medium-energy-resolution fluorescence detection mode. The undesired edge may arise either from another element present in the sample or actually from the same element that is being studied. An example for the former is Fe in protein samples where the active site containing Mn is studied. The Fe K-edge occurs in the Mn EXAFS range and limits the available *k*-range for EXAFS analysis. Using HERFD XAS the Fe K-edge can be eliminated and the Mn EXAFS analysis is greatly improved. The technique was successfully applied to study the oxygen evolving complex in the photosynthesis multi-protein complex photosystem II (PS II) [26]. The same principle was applied to rare earth elements to eliminate the L_1-edge in the L_2 EXAFS and the possibility of identifying multiple excitations in the EXAFS range has been discussed [27]. However, here the pathways of possible electronic transitions are more complex and difficulties were encountered caused by cascade decays that are expected to be even more pronounced at the L_3-edge. Range-extended EXAFS using HERFD requires the sample to be dilute like in standard fluorescence detected XAS [27].

5. Resonant X-ray emission spectroscopy

The incident energy can be tuned to an absorption feature near the Fermi level that arises from an excitation into a localized state. If the radiative decay of this resonantly excited state is detected with lifetime resolution it is referred to as RXES or RIXS. The sensitivity of RIXS to the electronic structure depends on the final state that is being detected [3].

The final state contains a core hole if the final state energy (energy transfer) is larger than a few tens of electron volts (cf. Fig. 1). For example, 1s2p RIXS has a 1s core hole in the intermediate state, i.e. a K-edge absorption feature, and a 2p hole in the final state. The 2p hole strongly interacts with the valence electrons in 3d transition metals and this interaction contains information about the valence electron configuration. The information is similar to L-edge absorption spectroscopy with the advantage of having the hard X-ray probe in 1s2p RIXS [5]. A comparison between the RIXS and the L-edge absorption spectra provides valuable insight into the character of electron–electron interactions and the interplay with ligand field splittings [14,28].

1s3p RIXS spectroscopy in 3d transition metals exhibits a strong spin-sensitivity in the final state and allows to record spin-selective absorption spectra [29,30]. This can be used to separate the K absorption pre-edge into spin-up and spin-down excitations and thus help to understand the origin of the spectral features [31,32]. Pirngruber et al. applied spin-selective spectroscopy to verify the presence and absence, respectively, of high-spin $3d^4$ configuration in $SrFeO_{3-x}$ and a Fe-ZSM-5 catalyst during reaction with N_2O [33,34].

The RIXS spectra become directly sensitive to the valence shell when the final state energy is only of a few electron volts as has been shown by many authors in particular in the soft X-ray region [35]. Fig. 6 shows the transition between core level RIXS and valence band RIXS for WO_2 and WO_3 with a formal $5d^2$ and $5d^0$ configuration, respectively. Along the diagonal direction, a crystal field splitting is visible for WO_3. The peaks split along the energy transfer direction in WO_2. This splitting is due to interactions between the 5d electrons (multiplets) and charge transfer. We thus observe dd and charge transfer excitations using an element-selective hard X-ray probe.

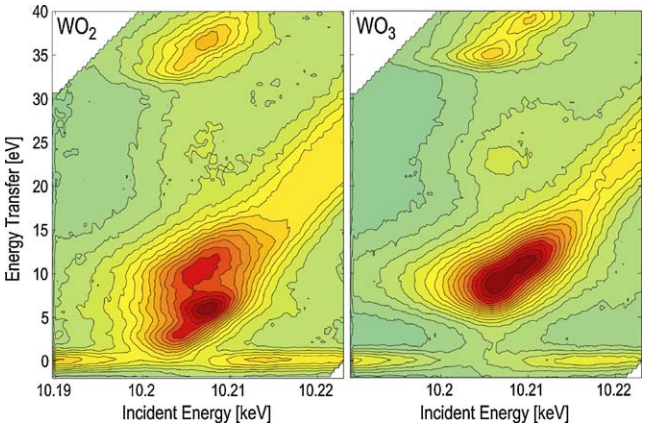

Fig. 6. Contour plots of the valence band RIXS in WO_2 and WO_3.

6. Conclusions

X-ray emission detection with lifetime resolution is a technique that is sensitive to the electronic structure and thus complementary to XAS. The experimental requirements with respect to sample environment are similar to XAS. An experimental setup should therefore ensure that both techniques can be applied simultaneously where XAS is measured either in transmission or in fluorescence detection mode. Sample characterization on an X-ray beamline will then be more complete and the data analysis will be more robust because the different spectra will also serve to validate the interpretation. X-ray emission spectrometers are currently being developed at various synchrotron radiation sources. It is desirable that these endstations will be installed permanently on XAS beamlines in order to minimize setup time and to make the technique readily available for users. With increasing user-friendliness in the operation and theoretical codes that provide options to calculate XES, more and more user groups will appreciate the benefits of XES and we assume that XES will become a standard technique.

Acknowledgments

We acknowledge the European Synchrotron Radiation Facility support groups and the staff of beamline ID 26.

References

[1] B.K. Teo, D.C. Joy (Eds.), EXAFS Spectroscopy. Techniques and Application, Plenum Press, New York, 1981.
[2] D.C. Koningsberger, R. Prins (Eds.), X-ray Absorption: Principles, Applications, Techniques of EXAFS, SEXAFS, and XANES, John Wiley & Sons, New York, 1988.
[3] F.M.F. de Groot, A. Kotani, Core Level Spectroscopy of Solids, Taylor and Francis, New York, 2008.
[4] A. Meisel, G. Leonhardt, R. Szargan, X-ray Spectra and Chemical Binding, Springer-Verlag, New York, 1989.
[5] P. Glatzel, U. Bergmann, Coord. Chem. Rev. 249 (2005) 65.
[6] H. Hayashi, M. Kawata, R. Takeda, Y. Udagawa, Y. Watanabe, T. Takano, S. Nanao, N. Kawamura, J. Electron Spectrosc. Relat. Phenom. 136 (2004) 191.
[7] U. Bergmann, S.P. Cramer, Crystal and Multilayer Optics, vol. 3448, SPIE, San Diego, 1998, p. 198.
[8] R. Verbeni, M. Kocsis, S. Huotari, M. Krisch, G. Monaco, F. Sette, G. Vanko, J. Phys. Chem. Solids 66 (2005) 2299.
[9] A. Kotani, S. Shin, Rev. Mod. Phys. 73 (2001) 203.

[10] P.W. Loeffen, R.F. Pettifer, S. Mullender, M.A. van Veenendaal, J. Rohler, D.S. Sivia, Phys. Rev. B 54 (1996) 14877.
[11] K. Hämäläinen, D.P. Siddons, J.B. Hastings, L.E. Berman, Phys. Rev. Lett. 67 (1991) 2850.
[12] P. Carra, M. Fabrizio, B.T. Thole, Phys. Rev. Lett. 74 (1995) 3700.
[13] W.M. Heijboer, P. Glatzel, K.R. Sawant, R.F. Lobo, U. Bergmann, R.A. Barrea, D.C. Koningsberger, B.M. Weckhuysen, F.M.F. de Groot, J. Phys. Chem. B 108 (2004) 10002.
[14] F.M.F. de Groot, P. Glatzel, U. Bergmann, P.A. van Aken, R.A. Barrea, S. Klemme, M. Havecker, A. Knop-Gericke, W.M. Heijboer, B.M. Weckhuysen, J. Phys. Chem. B 109 (2005) 20751.
[15] S. Huotari, T. Pylkkänen, G. Vankó, R. Verbeni, P. Glatzel, G. Monaco, Phys. Rev. B 78 (2008) 041102.
[16] G. Peng, F.M.F. Degroot, K. Hämäläinen, J.A. Moore, X. Wang, M.M. Grush, J.B. Hastings, D.P. Siddons, W.H. Armstrong, O.C. Mullins, S.P. Cramer, J. Am. Chem. Soc. 116 (1994) 2914.
[17] U. Bergmann, C.R. Horne, T.J. Collins, J.M. Workman, S.P. Cramer, Chem. Phys. Lett. 302 (1999) 119.
[18] V.A. Safonov, L.N. Vykhodtseva, Y.M. Polukarov, O.V. Safonova, G. Smolentsev, M. Sikora, S.G. Eeckhout, P. Glatzel, J. Phys. Chem. B 110 (2006) 23192.
[19] A. Mijovilovich, U. Bergmann, P. Glatzel, G. Parkin, P. Ellis, J.E. Penner-Hahn, manuscript in preparation.
[20] P. Glatzel, U. Bergmann, F.M.F. de Groot, S.P. Cramer, in: A. Bianconi, A. Marcelli (Eds.), X-ray and Inner-Shell Processes, vol. 652, American Institute of Physics, Rome, 2002, p. 250.
[21] F.M.F. de Groot, M.H. Krisch, J. Vogel, Phys. Rev. B 66 (2002) 195112.
[22] J.A. van Bokhoven, C. Louis, J.T. Miller, M. Tromp, O.V. Safonova, P. Glatzel, Angew. Chem. Int. Ed. 45 (2006) 4651.
[23] O.V. Safonova, M. Tromp, J.A. van Bokhoven, F.M.F. de Groot, J. Evans, P. Glatzel, J. Phys. Chem. B 110 (2006) 16162.
[24] H. Hayashi, Y. Udagawa, W.A. Caliebe, C.C. Kao, Chem. Phys. Lett. 371 (2003) 125.
[25] J.J. Rehr, R.C. Albers, Rev. Mod. Phys. 72 (2000) 621.
[26] J. Yano, Y. Pushkar, P. Glatzel, A. Lewis, K. Sauer, J. Messinger, U. Bergmann, V. Yachandra, J. Am. Chem. Soc. 127 (2005) 14974.
[27] P. Glatzel, F.M.F. de Groot, O. Manoilova, D. Grandjean, B.M. Weckhuysen, U. Bergmann, R. Barrea, Phys. Rev. B 72 (2005).
[28] P. Glatzel, U. Bergmann, J. Yano, H. Visser, J.H. Robblee, W.W. Gu, F.M.F. de Groot, G. Christou, V.L. Pecoraro, S.P. Cramer, V.K. Yachandra, J. Am. Chem. Soc. 126 (2005) 9946.
[29] K. Hämäläinen, C.C. Kao, J.B. Hastings, D.P. Siddons, L.E. Berman, V. Stojanoff, S.P. Cramer, Phys. Rev. B 46 (1992) 14274.
[30] X. Wang, F.M.F. deGroot, S.P. Cramer, Phys. Rev. B 56 (1997) 4553.
[31] P. Glatzel, A. Mirone, S.G. Eeckhout, M. Sikora, G. Giuli, Phys. Rev. B 77 (2008) 115133.
[32] H. Hayashi, M. Kawata, Y. Udagawa, N. Kawamura, S. Nanao, Phys. Rev. B 70 (2004).
[33] G.D. Pirngruber, J.D. Grunwaldt, P.K. Roy, J.A. van Bokhoven, O. Safonova, P. Glatzel, Catal. Today 126 (2007) 127.
[34] G.D. Pirngruber, J.D. Grunwaldt, J.A. van Bokhoven, A. Kalytta, A. Reller, O.V. Safonova, P. Glatzel, J. Phys. Chem. B 110 (2006) 18104.
[35] S.M. Butorin, J.H. Guo, M. Magnuson, P. Kuiper, J. Nordgren, Phys. Rev. B 54 (1996) 4405.